Phase unwrapping from measured phase differences for optical wave propagating through the turbulent atmosphere

V.A. Banakh and A.V. Falits

Institute of Atmospheric Optics,
Siberian Branch of the Russian Academy of Sciences, Tomsk

Received September 29, 2000

The algorithm for phase unwrapping from the principal value of the phase gradient is proposed. The efficiency of this algorithm is studied using, as an example, adaptive focusing of an optical wave propagating through the turbulent atmosphere under conditions of strong scintillations of intensity.

Introduction

Numerous problems of interferometry, image restoration, and adaptive optics involve reconstruction of a wave phase (phase unwrapping) either from its principal value or from the gradient of its principal value. In the first case, for example, for interferometric synthetic aperture radars (SAR), the phase unwrapping problem[1–3] is formulated as follows: to find the estimate $\hat{\varphi}(i, k)$ of the 2D phase $\varphi(i, k)$ given by its principal value $\psi(i, k)$

$$\psi(i, k) = P[\varphi(i, k)] = \varphi(i, k) \pm 2\pi n, \qquad (1)$$

where i and k determine the pixel location in a 2D array of discrete phase values, the operator $P[\ldots]$ means reduction of the function in the brackets to the interval $[-\pi, \pi]$ of the phase principal value.

The true value of the phase cannot be reconstructed without recourse to some assumptions, and we have a trivial solution $\hat{\varphi} = \psi$. Therefore, to obtain the estimate $\hat{\varphi}$, it is usually assumed that the phase φ has no discontinuities, i.e., its values at neighboring nodes of the discrete grid differ by no more than $\pm\pi$. It can be shown that in this case the gradient of the principal phase value $\hat{\nabla}\psi$ limited by its principal value coincides with the gradient of the true phase $\nabla\varphi$ (Ref. 2):

$$\hat{\nabla}\psi(i, k) = \nabla\varphi(i, k), \qquad (2)$$

where

$$\hat{\nabla}\psi(i, k) = \begin{pmatrix} P[\psi(i+1, k) - \psi(i, k)] \\ P[\psi(i, k+1) - \psi(i, k)] \end{pmatrix}. \qquad (3)$$

The true phase can be found from $\nabla\varphi$ by integrating $\hat{\nabla}\psi$ along an arbitrary path.

The situation changes in the presence of strong phase noise and violence of the condition $< \pm\pi$ imposed on the phase difference between neighboring nodes. Then the field of the gradient $\hat{\nabla}\psi$ ceases to be conservative

$$\hat{\nabla}\psi \neq \nabla\varphi$$

and includes a solenoid component

$$\nabla \times \hat{\nabla}\psi \neq 0, \qquad (4)$$

and the result of integration of $\hat{\nabla}\psi$ begins to depend on the selected path of unwrapping.

In the theory of interferometric SAR, two methods are largely used for determining the phase φ: the branch-cut method[1,3] and the least squares method (LSM).[2,3] In the branch-cut method, regions with $\hat{\nabla}\psi \neq \nabla\varphi$ are identified in interferograms, and the unwrapping path is selected so as to bypass these regions. The solution obtained in such a way is ambiguous and depends on the way of cutting.[3] In the least squares method, the difference between $\hat{\nabla}\psi$ and $\nabla\varphi$ is treated as a noise

$$\hat{\nabla}\psi = \nabla\varphi + \mathbf{n}_\nabla$$

and the estimate of the true phase is sought by minimizing the square form

$$\sum_i \sum_k |\nabla\hat{\varphi}(i, k) - \hat{\nabla}\psi(i, k)|^2. \qquad (5)$$

The variational problem (5) is equivalent to the finite-difference representation of the Poisson equation

$$\nabla \cdot \nabla\hat{\varphi} = \nabla \cdot \hat{\nabla}\psi \qquad (6)$$

with the Neumann boundary conditions. The solution of this equation and, consequently, the least squares method of estimating the true phase can be readily implemented on a uniform grid with the use of Fourier transform.[4] The boundary conditions in Eq. (6) for phase differences are set with the help of periodic extrapolation of the sought function beyond the domain of definition by mirror reflection of the initial grid function to the double-dimension grid.[4,12,16]

The problem of phase unwrapping from the principal (wrapped) value of the gradient of the wrapped phase arises when using interferometric or Hartman sensors to measure the wave phase front in

0235-6880/01/05 383-08 $02.00

adaptive optics systems. In the discrete representation, the phase gradient is written as

$$\mathbf{g}(i, k) = \frac{P[\psi(i+1, k) - \psi(i, k)]}{d}\,\mathbf{e}_x + \frac{P[\psi(i, k+1) - \psi(i, k)]}{d}\,\mathbf{e}_y, \quad (7)$$

where d is the distance between neighboring grid nodes; $\mathbf{e}_x$ and $\mathbf{e}_y$ are unit vectors. However, if the field of the phase gradient is nonconservative, then the least squares method, being usually applicable to phase estimation by difference of phases determined from local slopes, leads to some loss of useful information on the phase, because in this case the method does not allow the solenoidal component of the phase gradient (4) to be taken into account and the so-called hidden phase to be reconstructed.[5]

Actually, if we represent the vector field of the phase gradient $\mathbf{g}$ as a sum of the potential $\mathbf{g}_p$ and solenoidal $\mathbf{g}_s$ components and then apply the divergence operator to it,[6] then the solution (5) of the resulted Poisson equation (6) corresponds only to the potential part of the field $\mathbf{g}$: $\nabla\hat{\varphi} = \mathbf{g}_p$. In this paper, we propose the algorithm for phase unwrapping from the wrapped phase gradient and study the efficiency of this algorithm using, as an example, adaptive focusing of the optical wave propagating through the turbulent atmosphere under conditions of strong intensity scintillations.

1. Algorithm of the hidden phase unwrapping

The conservativeness of the field of the optical wave phase gradient (4) is violated in the turbulent atmosphere because of random distortions of the wave field at the medium inhomogeneities, which lead to the loss of spatial coherence and give rise to intensity scintillations. At long-distance propagation of the optical radiation, scintillations of the intensity become strong,[7] and a speckle structure arises in the plane transverse to the propagation direction. This structure includes areas with zero light intensity, and the phase becomes discontinued and having spiral singularities (branchpoints) called wavefront dislocations.[8] The characteristic feature of a dislocation at some point is that the principal value of the phase gradient changes by $\pm 2\pi$ when passing around this point by a closed loop. Thus, using Eq. (7), we can write[5]:

$$\mathbf{g}(i, k)\cdot\mathbf{e}_x d + \mathbf{g}(i+1, k)\cdot\mathbf{e}_y d - \mathbf{g}(i, k+1)\cdot\mathbf{e}_x d - \mathbf{g}(i, k)\cdot\mathbf{e}_y d = \begin{cases}\pm 2\pi, \text{ if a branchpoint is inside the loop},\\ 0, \text{ if there is no branchpoint inside the loop.}\end{cases} \quad (8)$$

Positive and negative branchpoints arise in pairs and are connected with each other through discontinuities of the phase surface in the areas with low wave intensity.

In the case of continuous functions, using the Stokes theorem, Eq. (8) can be rewritten as

$$\oint_C \mathbf{g}(\mathbf{r})\,d\mathbf{r} = \int_D d\mathbf{r}\,\mathbf{e}_z\cdot\nabla\times\mathbf{g}(\mathbf{r}) = \begin{cases}\pm 2\pi, \text{ if a branchpoint is inside the loop},\\ 0, \text{ if there is no branchpoint inside the loop},\end{cases} \quad (9)$$

where C denotes the boundary of the surface D. The loop C around a branchpoint can be selected arbitrary small, and the integrand in Eq. (9) can be approximated as[4]:

$$\mathbf{e}_z\cdot\nabla\times\mathbf{g}(\mathbf{r}) = \pm 2\pi\delta(\mathbf{r} - \mathbf{r}_{bp}), \quad (10)$$

where the vector $\mathbf{r}_{bp}$ determines the phase branchpoint.

Representing the phase gradient in the form

$$\mathbf{g}(\mathbf{r}) = \mathbf{g}_p(\mathbf{r}) + \mathbf{g}_s(\mathbf{r}) \quad (11)$$

and applying the rotor operator to it

$$\nabla\times\mathbf{g}(\mathbf{r}) = \nabla\times\mathbf{g}_s(\mathbf{r}), \quad (12)$$

we find that violation of the conservativeness of the phase gradient field is connected with nonzero rotor of the solenoidal gradient component.[2,9,5]

From Eqs. (10) and (12) it follows that

$$\mathbf{e}_z\cdot\nabla\times\mathbf{g}_s(\mathbf{r}) = \pm 2\pi\delta(\mathbf{r} - \mathbf{r}_{bp}). \quad (13)$$

Represent the estimate of the true phase in the form[5]

$$\hat{\varphi}(\mathbf{r}) = \hat{\varphi}_{lsme}(\mathbf{r}) + \hat{\varphi}_{hid}(\mathbf{r}), \quad (14)$$

where $\hat{\varphi}_{lsme}(\mathbf{r})$ is the estimate of the true phase by the least squares method (5), which corresponds to the potential component of the phase gradient $\mathbf{g}_p$; $\hat{\varphi}_{hid}(\mathbf{r})$ is the hidden phase determined by the solenoidal phase component $\mathbf{g}_s$. Applying the gradient operator to the right- and left-hand sides of Eq. (14), with allowance for Eqs. (11) and (13), we have

$$\nabla\times\nabla\hat{\varphi}_{hid}(\mathbf{r}) = \pm 2\pi\delta(\mathbf{r} - \mathbf{r}_{bp})\mathbf{e}_z. \quad (15)$$

The solution of this equation is presented in Ref. 5; it has the form

$$\hat{\varphi}_{hid}(\mathbf{r}) = \mathrm{Im}\{\pm\log[(x - x_{bp}) + i(y - y_{bp})]\}. \quad (16)$$

In the general case, keeping in mind that positive and negative branchpoints arise in pairs, for $\hat{\varphi}_{hid}$ we have[5]:

$$\hat{\varphi}_{hid}(\mathbf{r}) = \mathrm{Im}\left\{\log\left[\frac{\prod_{k=1}^{K}(x - x_k) - i(y - y_k)}{\prod_{k=1}^{K}(x - x'_k) - i(y - y'_k)}\right]\right\}, \quad (17)$$

where x_k, y_k and x'_k, y'_k are respectively the coordinates of positive and negative phase branchpoints; K is the number of pairs.

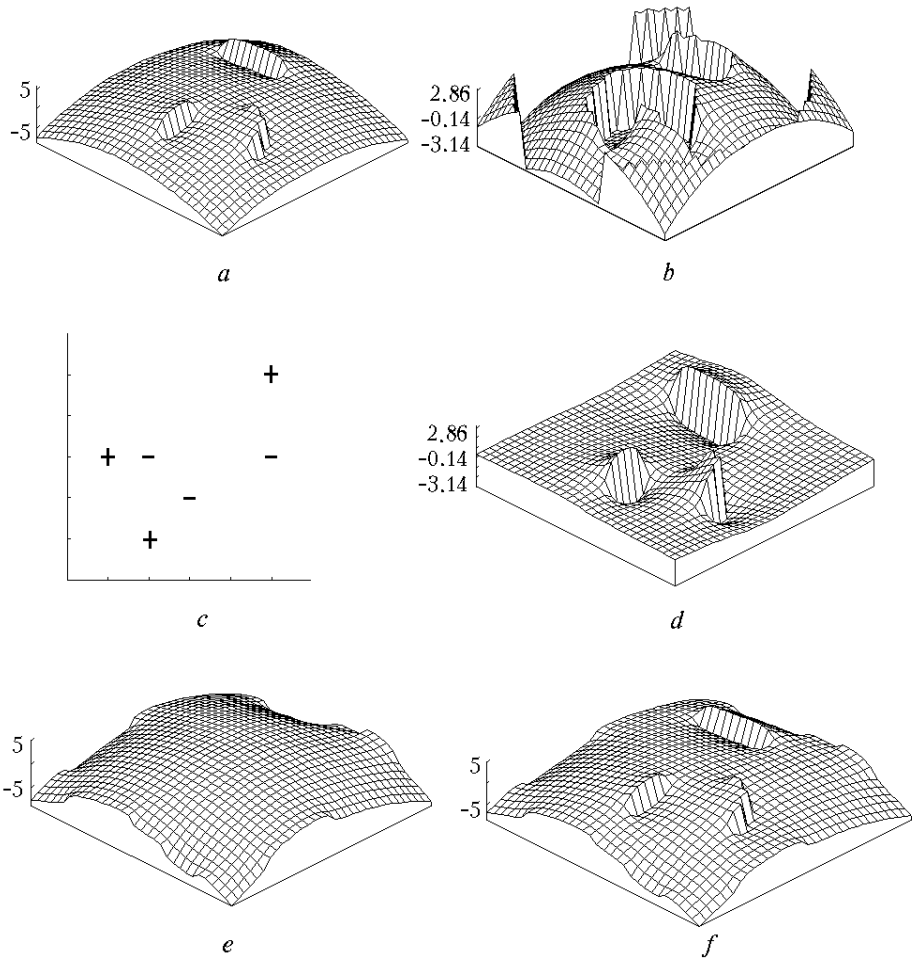

Fig. 1. Phase estimated by the least squares method with allowance for the hidden phase.

Figure 1 illustrates the performance of the least squares method in phase unwrapping. Figure 1*a* shows the phase function having discontinuities, and Fig. 1*b* shows the principal value of the true phase described by Eq. (1). Calculating the loop integral (8), we can find three pairs of phase branchpoints, whose location is shown in Fig. 1*c*. The hidden phase (Fig. 1*d*) is calculated by Eq. (17). The phase estimate by the least squares method is shown in Fig. 1*e*. The phase constructed as a sum of $\hat{\varphi}_{\text{lsme}}$ in Fig. 1*e* and $\hat{\varphi}_{\text{hid}}$ in Fig. 1*d* by Eq. (14) is shown in Fig. 1*f*.

2. Reconstruction of the hidden phase

2.1. Formulation of the problem of numerical simulation

The efficiency of the above-described phase unwrapping algorithm was studied, using adaptive focusing of a wave propagating through the turbulent atmosphere as an example. The problem was considered in the following formulation. A collimated light beam with the Gauss amplitude distribution in the initial plane propagates through the atmosphere. The turbulent conditions of propagation are characterized by the parameter

$$\beta_0^2 = 1.23\, C_n^2\, k^{7/6} L^{11/6}, \qquad (18)$$

where C_n^2 is the structure characteristic of fluctuations of the air refractive index, $k = 2\pi/\lambda$ is the wave number, λ is the wavelength, L is the path length. The parameter β_0^2 is the dispersion of intensity scintillations (scintillation index) of the plane wave. It is calculated in the first approximation of the method of smooth perturbations.[10] This parameter is widely used as a unit of the intensity of optical turbulence.[7] The path terminates in a collecting lens, in front of which is situated a phase corrector.

The numerical experiment on focusing the radiation passed through a layer of a turbulent medium was conducted for different schemes of correction of phase distortions: ideal phase conjugation that instantaneously and exactly reconstructs the wave phase; compensation for distortions of the phase reconstructed by the least squares method from phase differences; the correction based on the phase unwrapping by the least squares method from phase differences with allowance for the hidden phase; and,

finally, absence of phase correction. The efficiency of phase correction is estimated by the Strehl ratio

$$\mathrm{St} = I/I_0, \qquad (19)$$

which is the ratio of light intensity at the lens focus for a beam propagating through a turbulent (I) to the homogeneous medium (I_0). The scheme of the numerical experiment is shown in Fig. 2.

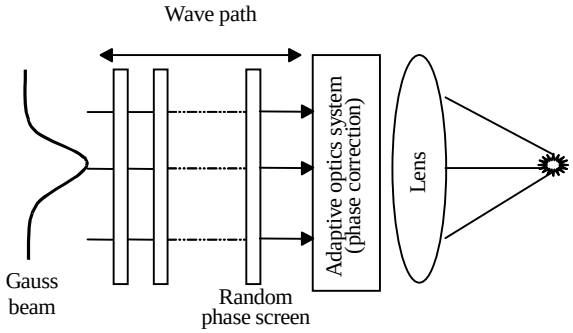

Fig. 2. Simulated adaptive focusing of the wave passed through a homogeneous turbulent layer.

Propagation of the light beam through the turbulent medium was simulated by solving numerically the parabolic equation

$$2ik\frac{\partial U(z,\rho)}{\partial z} + \Delta_\perp U(z,\rho) + 2k^2\tilde{n}(z,\rho)U(z,\rho) = 0, \qquad (20)$$

where $U(z,\rho)$ is the complex amplitude of the field; $\rho = (x, y)$; $\Delta_\perp = \frac{\partial^2}{\partial x^2} + \frac{\partial^2}{\partial y^2}$; $\tilde{n}$ is the fluctuating part of the refractive index; the beam propagates along the axis z. The beam path was divided into layers each having the thickness Δz. A random phase screen was modeled at the front boundary of every layer. Having passed through this screen, the beam acquired phase distortions. Then the beam diffraction inside every layer was calculated with the use of the fast Fourier transform.

The phase screen was modeled by the following equation:

$$\theta(j\Delta x, l\Delta y) = \sum_{n=0}^{N_x}\sum_{m=0}^{N_y}[a(n,m) + ib(n,m)]\left[2\pi i\left(\frac{jn}{N_x} + \frac{lm}{N_y}\right)\right], \qquad (21)$$

where Δx and Δy are the distances between the nodes of the computational grid along the coordinates x and y; N_x and N_y are array dimensions; $L_x = \Delta x N_x$ and $L_y = \Delta y N_y$ are dimensions of the computational grid; $a(n,m)$ and $b(n,m)$ are random uncorrelated series with the variance

$$\langle a^2(n,m)\rangle = \langle b^2(n,m)\rangle = \Delta q_x \Delta q_y \Phi_\theta(n\Delta q_x, m\Delta q_y, z),$$

where Φ_θ is the spectral density of phase fluctuations; $\Delta q_x = \frac{2\pi}{N_x\Delta x}$ and $\Delta q_y = \frac{2\pi}{N_y\Delta y}$ determine the grid step in the spectral region. The spectrum of phase fluctuations is given by the equation

$$\Phi_\theta(q_x, q_y, q_z) = 2\pi k^2 \Delta z \Phi_n(q_x, q_y, q_z = 0, z), \qquad (22)$$

where

$$\Phi_n(q) = 0.033\, C_n^2\, q^{-11/3} \exp(-q^2/q_\mathrm{m}^2) \qquad (23)$$

is the spectrum of turbulent fluctuations of the refractive index; $q = |\mathbf{q}|$, $q_\mathrm{m} = 5.92/l_0$, l_0 is the inner scale of turbulence.

The algorithm of the phase screen modeling (21) does not allow us to account correctly for the frequencies lower than the value determined by the grid step in the frequency region Δq_x and Δq_y. This leads to errors in modeling of large-scale phase fluctuations. Therefore, for modeling the phase screen near the zero frequency, we used the method of subharmonics.[11] According to this method, the equation for θ has the form

$$\theta_\mathrm{sh}(j\Delta x, l\Delta y) = \sum_{p=1}^{N_p}\sum_{n=-1}^{1}\sum_{m=-1}^{1}[a(n,m,p) + ib(n,m,p)] \times \left[2\pi i\frac{jn}{3^p N_x} + 2\pi i\frac{lm}{3^p N_y}\right], \qquad (24)$$

where $\langle a^2(n,m,p)\rangle = \langle b^2(n,m,p)\rangle = \Delta q_{x_p}\Delta q_{y_p}\Phi_\theta(n\Delta q_{x_p}, m\Delta q_{y_p})$, $n \neq 0$, $m \neq 0$. In modeling, we took $N_p = 3$, and the grid step was determined by $\Delta q_{x_p} = \frac{\Delta q_x}{3^p}$ and $\Delta q_{y_p} = \frac{\Delta q_y}{3^p}$.

2.2. Hidden phase and efficiency of adaptive focusing

The effect of the hidden phase on the efficiency of phase correction was studied in Refs. 12–16, where it was concluded that the efficiency of adaptive systems decreases markedly if the correction technique ignores the "vortex" component of the phase. However, in Refs. 12–14 and 16 the vortex component itself was not reconstructed from the phase differences measured by wavefront sensors. What's more, in Refs. 12 and 14 it was noted that the attempts to account for the hidden phase from the phase differences using the algorithms from Ref. 4 failed. Unlike Refs. 12–14 and 16, our calculations of the adaptive focusing efficiency are based on the results of reconstruction of the hidden phase with the use of the above algorithm, and they are obtained in a wider range of values of the parameter β_0^2.

Figure 3 shows the plots of the Strehl ratio as a function of the scintillation index (18) for the case of a plane wave propagating in the turbulent atmosphere. Figure 4 shows the similar results for the collimated Gaussian beam with the Fresnel number of the transmitting aperture $\Omega = ka^2/L$ ranging from 90 to 4.5, where a is the initial beam radius.

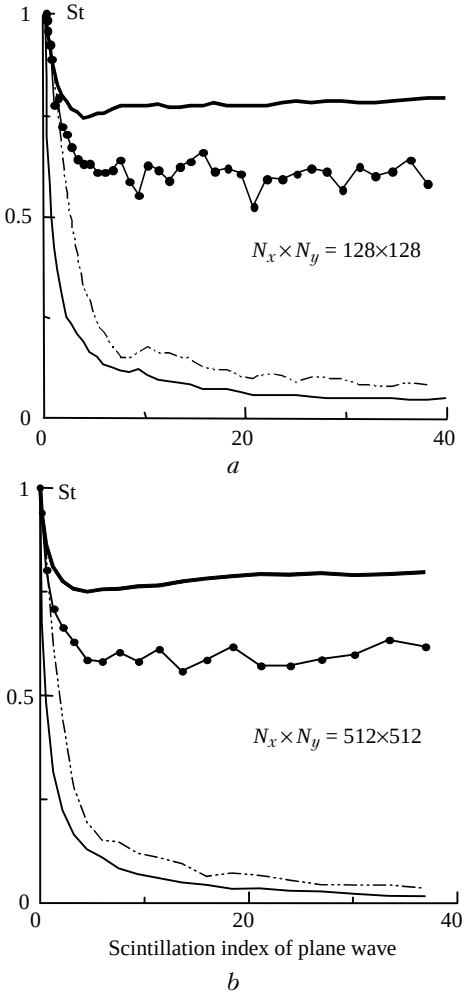

Fig. 3. Strehl ratio as a function of the scintillation index at plane wave focusing: no phase correction (———), ideal phase correction (———), LSM correction (— · · —), correction with allowance for the hidden phase (—●—●—).

It is seen from Figs. 3 and 4 that allowance for the hidden phase in the phase unwrapping improves the efficiency of the adaptive focusing in the region of strong intensity scintillations $\beta_0^2 > 2$ in the case that the density of dislocations increases markedly as compared to the phase unwrapping by the least squares method. If the efficiency of adaptive focusing based on the phase unwrapping by the least squares method decreases as the turbulence (parameter β_0^2) on the path increases, then the allowance for the hidden phase keeps the Strehl ratio in the region of strong fluctuations at roughly the same level. In the case of a collimated beam, the allowance for the hidden phase gives the results for the Strehl ratio that almost coincide with the results given by an ideal phase corrector. This points to the high efficiency of the implemented phase unwrapping algorithm.

Locations of the branchpoints in the phase distribution were sought according to Eq. (8) by summing phase differences (gradients) along the path determined by the step of the computational grid. The phase was estimated by Eqs. (5), (14), and (17). From comparison of the results calculated at $N_x = N_y = 128$ and 512 and shown in Figs. 3 and 4, it follows that the pattern keeps qualitatively the same as the step of the computational grid changes.

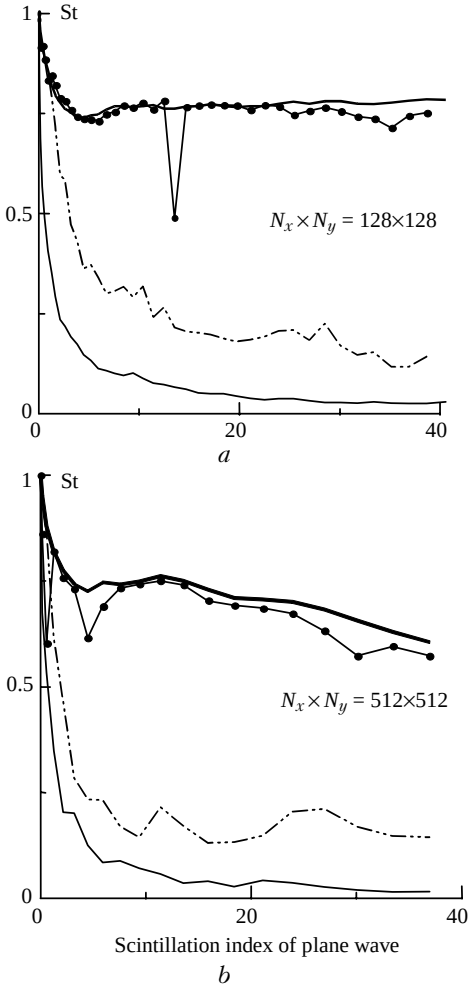

Fig. 4. Strehl parameter as a function of the scintillation index at Gaussian beam focusing: no phase correction (———), ideal phase correction (———), LSM correction (— · · —), correction with allowance for the hidden phase (—●—●—).

Nevertheless, the phase unwrapping algorithm not always gives good results. It is seen from Fig. 4 for the curves corresponding to the Strehl ratio in the case of correcting the phase reconstructed by the least squares method with allowance for the hidden phase, where some points lie significantly lower than others. Let us dwell on possible causes of such discrepancies.

2.3. False cuts

If the principal value of the phase ψ is known, for example, from the results of numerical solution of Eq. (20) for the complex amplitude of the field, then the hidden phase can be calculated as

$$\hat{\varphi}_{\text{hid}} = P\,[\,\psi - \hat{\varphi}_{\text{lsme}}]\,. \qquad (25)$$

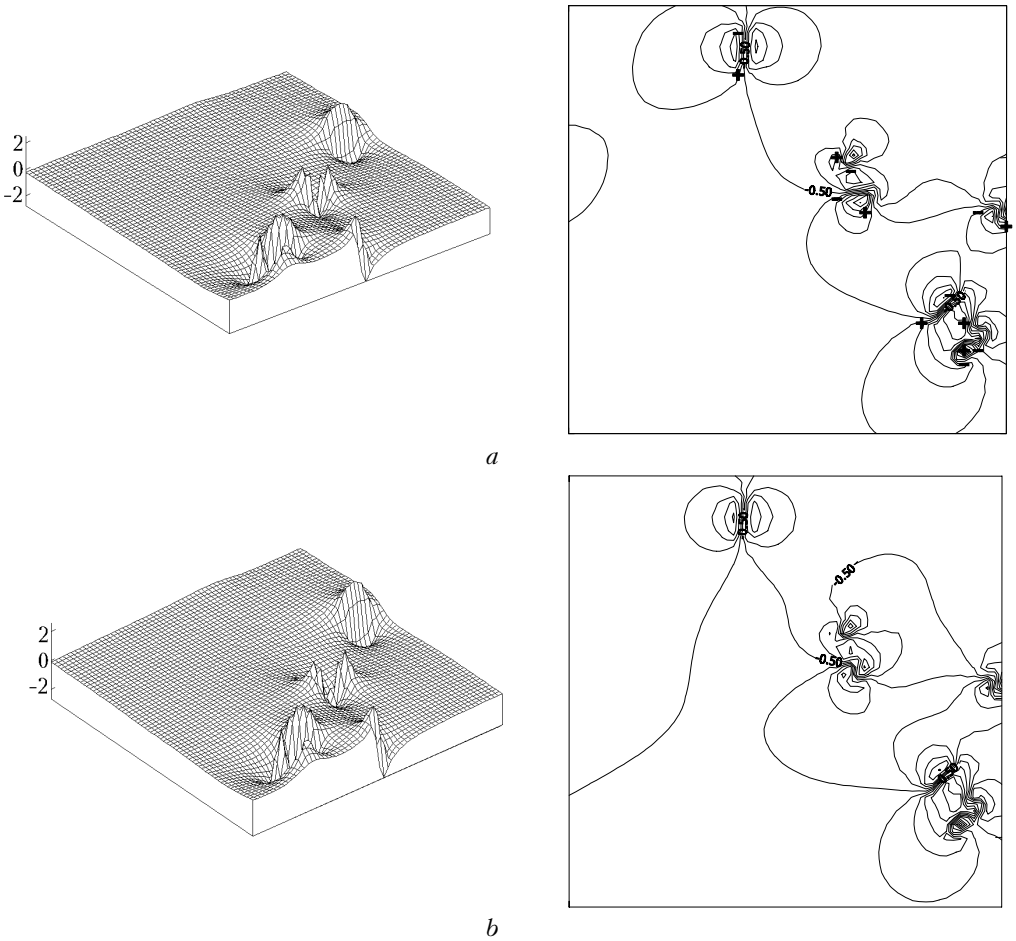

Fig. 5. True hidden phase and location of phase branchpoints (*a*) and hidden phase calculated from the determined branchpoints (*b*).

The hidden phase thus determined was compared with the hidden phase calculated by Eq. (17). The efficiency of adaptive focusing with the algorithm employing Eq. (25) proves to be just the same as in the case of ideal phase correction. Figure 5 shows the hidden phase and its profile calculated by Eqs. (25) and (17).

It is seen from Fig. 5 that for this example the both approaches give almost the same results. So, the calculated efficiency of adaptive focusing with the use of Eq. (17) accounting for the hidden phase is close to the efficiency of focusing with the use of an ideal corrector. However, this is not always the case.

The point is that the hidden phase is reconstructed from the coordinates of positive and negative branchpoints. When seeking the branchpoints, the integration loop in Eq. (8) cannot be taken infinitely small – it always has finite size determined by the grid step. As a result, reconstruction of the hidden phase by Eq. (17) can introduce an error. Figure 6 shows schematically the situations, which may arise when determining the coordinates of the phase branchpoints.

It is seen from Fig. 6 that if both the negative and positive branchpoints are inside the loop A, then the loop integral equals zero and the both branchpoints cannot be detected. So, the algorithm for detection of branchpoints gives an error. This error can be neglected, if the loop contains paired points connected by a phase cut, because the length of this cut is short.

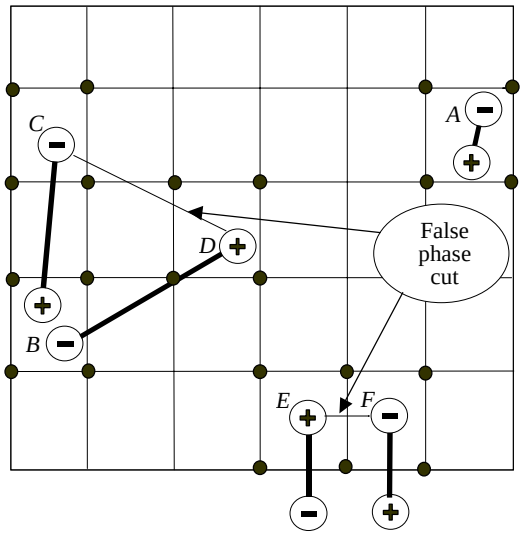

Fig. 6. Scheme of possible formation of false cuts when calculating the hidden phase by Eq. (17).

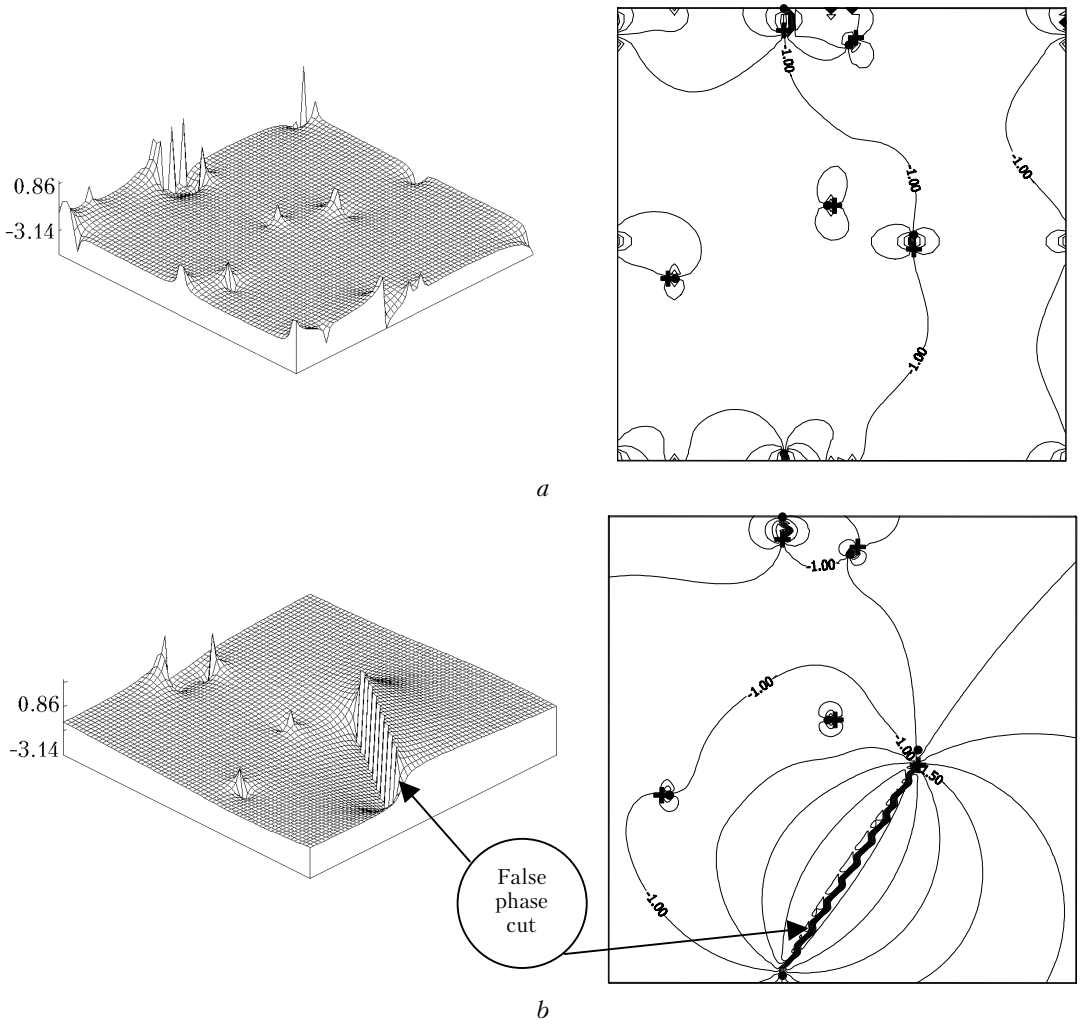

Fig. 7. Formation of false phase cuts: true hidden phase (*a*) and hidden phase with a false phase cut (*b*).

The loop *B* also contains two phase branchpoints, but they are not connected by a phase cut. The loop integral in this case is also zero. When calculating the hidden phase, the negative point inside the loop *C* is connected by the phase cut with the positive point inside the loop *D*. Thus, a false phase discontinuity is reconstructed.

Paired points may also be located beyond the computational grid. The point in the loop *E* is connected with the point located beyond the domain of consideration. The situation with the point inside the loop *F* is just similar. When calculating by Eq. (17), the positive phase branchpoint in the loop *E* is connected by a false cut with the point inside the loop *F*. If the number of such false discontinuities is large enough, then the hidden phase calculated by Eq. (17) may differ widely from the result given by Eq. (25).

In numerical simulation, the above situations connected with appearance of false phase cuts can be traced. Figure 7*a* shows the hidden phase and its profile with branchpoints found according to Eq. (25). Figure 7*b* shows the surface and profile of the hidden phase calculated by Eq. (17) using the found branchpoints. It is clearly seen where the hidden phase found by Eq. (17) coincides with the true hidden phase and where the false phase cut is located.

Conclusion

In this work, we have implemented the algorithm of phase unwrapping from the principal value of the phase gradient and examined its efficiency using, as an example, adaptive focusing of a wave propagating through the turbulent atmosphere under conditions of strong scintillations of intensity. Despite the fact that false phase cuts may sometimes be formed when using this algorithm, its efficiency is high on the average.

The accuracy of this algorithm can be improved. For example, decreasing the distance between the nodes of the computational grid (increasing the resolution) we can decrease the number of false phase discontinuities. The error connected with boundary points can be eliminated by excluding unpaired points from calculation of the hidden phase by Eq. (17).

Acknowledgments

The authors would like to express their gratitude to I.N. Smalikho for his help in development of the numerical simulation algorithm of wave propagation in the turbulent atmosphere.

References

1. R.M. Goldstein, H.A. Zebker, and C.L. Werner, Radio Sci. **23**, No. 4, 713–720 (1988).
2. R. Bamler, N. Adam, G. Davidson, and D. Just, IEEE Trans. Geosci. Remote Sens. **36**, No. 3, 913–921 (1998).
3. D.C. Ghiglia, and M.D. Pritt, *Two-Dimensional Phase Unwrapping: Theory, Algorithms, and Software* (Wiley Interscience, New York, 1998), 492 pp.
4. H. Takajo and T. Takahashi, J. Opt. Soc. Am. A **5**, No. 3, 416–425 (1988).
5. D.L. Fried, J. Opt. Soc. Am. A **15**, No. 10, 2759–2768 (1998).
6. J. Herrman, J. Opt. Soc. Am. **70**, No. 1, 28–35 (1980).
7. V.E. Zuev, V.A. Banakh, and V.V. Pokasov, *Optics of the Turbulent Atmosphere* (Gidrometeoizdat, Leningrad, 1988), 270 pp.
8. N.B. Baranova, A.V. Mamaev, N.F. Pilipetsky, V.V. Shkunov, and B.Ya. Zel'dovich, J. Opt. Soc. Am. **73**, No. 5, 525–528 (1983).
9. V. Aksenov, V. Banakh, and O. Tikhomirova, Appl. Opt. **37**, No. 21, 4536–4540 (1998).
10. V.I. Tatarskii, *Wave Propagation in a Turbulent Medium* (McGraw Hill, New York, 1968).
11. R. Frehlich, Appl. Opt. **39**, No. 3, 393–397 (2000).
12. V.P. Lukin and B.V. Fortes, Atmos. Oceanic Opt. **8**, No. 3, 223–230 (1995).
13. B.V. Fortes, Atmos. Oceanic Opt. **12**, No. 5, 406–411 (1999).
14. V.P. Lukin and B.V. Fortes, Atmos. Oceanic Opt. **13**, No. 5, 478–483 (2000).
15. M.C. Roggemann, and A.C. Koivunen, J. Opt. Soc. Am. A **17**, No. 5, 911–919 (2000).
16. V.P. Lukin and B.V. Fortes, *Adaptive Formation of Beams and Images in the Atmosphere* (SB RAS Publishing House, Novosibirsk, 1999), 214 pp.